

An Experimental Approach to Vibro-Acoustic Study of Beam-Type Structures

Jeniffer TORRES-ROMERO⁽¹⁾, William CARDENAS⁽²⁾, Jesus CARBAJO⁽³⁾
Enrique G. SEGOVIA EULOGIO⁽⁴⁾, Jaime RAMIS-SORIANO⁽³⁾

⁽¹⁾ *Institute of Applied Physics Science and Technology*
University of Alicante
Spain; e-mail: jtr17@alu.ua.es

⁽²⁾ *Klippel GmbH*
e-mail: w.cardenas@klippel.de

⁽³⁾ *Department of Physics, System Engineering and Signal Theory*
University of Alicante
Spain; e-mail: {jesus.carbajo, jramis}@ua.es

⁽⁴⁾ *Department of Civil Engineering, University of Alicante*
Spain; e-mail: enrique.gonzalo@ua.es

(received September 19, 2017; accepted January 24, 2018)

In this paper an alternative procedure to vibro-acoustics study of beam-type structures is presented. With this procedure, it is possible to determine the resonant modes, the bending wave propagation velocity through the study of the radiated acoustic field and their temporal evolution in the frequency range selected. As regards the purely experimental aspect, it is worth noting that the exciter device is an actuator similar to is the one employed in distributed modes loudspeakers; the test signal used is a pseudo random sequence, in particular, an MLS (Maximum Length Sequence), facilitates post processing. The study case was applied to two beam-type structures made of a sandstone material called Bateig. The experimental results of the modal response and the bending propagation velocity are compared with well-established analytical solution: Euler-Bernoulli and Timoshenko models, and numerical models: Finite Element Method – FEM, showing a good agreement.

Keywords: beam; modal shape; modal analysis; MLS; bending wave propagation velocity.

1. Introduction

The effects of structural vibrations on the acoustic field in the neighbouring acoustic fluids have been key issues in several engineering fields (CROCKER, 2007). Sound-structure interaction is an important topic for the acoustician and noise control engineers. Since beams and plates are basic in engineering and construction fields, it is of utmost importance to have not only analytic, numeric and experimental tools at our disposal but also the means to analyse and quantify the influence of significant parameters in noise and vibration control applications (GERGES, ARENAS, 2010).

Any structure when subjected to dynamic loads vibrates and radiates sound in a frequency range that depends on its mechanical and geometrical properties.

The acoustic radiation efficiency, however, depends on frequency. Below the so-called critical frequency, the radiation is negligible and above it, the radiation is highly efficient (CROCKER, 2007; GERGES, ARENAS, 2010). Therefore, the analysis of these parameters is of great importance in noise and vibrations control applications (EWINS, 1984).

This study of the effects of structural vibrations on the acoustic field requires careful inspection and testing. For modal analysis, we apply one of the most widely used measurement techniques, the so-called mobility measurements. The system is tested by means of a Transfer Function Velocity vs Force. The load force applied to excite the structure may be either stationary (produced by a modal exciter or shaker) or transitory (by an impact hammer) (EWINS, 1984). The excita-

tion force is captured by a force sensor and the system's dynamic response in the selected receiver point registered by piezoelectric sensors sensitive to acceleration (accelerometers). The mass of the transducers, the emitter and especially that of the receiver, must be significantly lower than that of the moving assembly so as to minimize its influence on the system's vibrational behaviour (EWINS, 1984).

However, this type of measurement is characterized by some limitations: the measurement in the transient or impulsive mode shows inaccuracies inherent to the application of the force, and the low coherence and low signal-to-noise ratio in the stationary mode tends to degrade the measured data. If the mechanical excitation uses an electrodynamic shaker, particular attention has to be paid to the way in which the shaker and structure are connected and to the noise radiated by the shaker itself as this may contaminate the measured sound. There are, in fact, difficulties in exciting a structure with an electromechanical shaker, in particular at higher frequencies. Mass loading may occur due to the force transducer and its mounting arrangement; a stinger should be used to connect the shaker to the structure to avoid moment excitation. This has to be as straight as possible to avoid misalignment and to obtain the correct transmission of force. Finally, dynamic coupling between the shaker and the structure may occur affecting the force spectrum. In summary, the effectiveness of force transmission from the shaker to the structure decreases with increasing frequency, especially when a stinger is used. The interested reader will find a good discussion on this subject in (MCCONNELL, 2000)

Since its presentation, almost four decades ago, this measurement technique based on the use of pseudorandom sequences such as Maximum-Length Sequences (MLS) has been used to characterize linear time-invariant (LTI) systems, especially within the fields of room acoustics and electro-acoustics (SCHROEDER, 1979; VANDERKOOY, 1994; RIFE, VANDERKOOY, 1989; VÖRLANDER, KOB, 1997). MLS is the sequence most commonly used to obtain the system's impulse response (IR), even though other existing pseudorandom sequences that use correlation methods, such as the binary pseudorandom noises (PRN) or Chirp signals (MAZUREK, LASOTA, 2007), are applied. One of the key benefits of this technique is its high signal-to-noise ratio, which allows measurements in noisy areas using low-power testing signals.

The main aim of this paper is to present an alternative approach to determine the mechanical characteristics of beam-type structures and the characterization of its radiated acoustic field when subjected to a mechanical excitation. The experimental technique proposed allows obtaining the resonant modes of the beam and determining bending wave propagation velocity in the solid in function of the frequency. This is

achieved by analysing the sound pressure field close to the beam in the frequency and wave number, k , domain.

From the system impulse response analysis performed at the measurement points, the resonant modes of the beam and bending wave propagation velocity in the solid can be estimated. This approach, as explained below, affords the possibility to perform a temporary analysis of the structure and observe the interaction with the fluid surrounding it (MAO, PIETRZKO, 2013).

Our main interest in this paper is to show an alternative approach to establishing a correlation between structural vibrations and radiated sound from a practical perspective. Now then, our experiment consists in applying a mechanical exciter on a beam-type structure to determine its mechanical properties and its radiated acoustic field. We study the sound pressure field close to the beam in the frequency domain to describe the mechanical properties and calculate the flexural wave wavelength of the solid to delimit its radiated acoustic field. Given that the bending waves are responsible for sound radiation (FAHY, GARDONIA, 2007), our approach, unlike those that use contact sensors, renders unnecessary to implement signal processing strategies to quantify the contribution of the different kinds of waves propagated over the structure (SZWERC *et al.*, 2000; LINJAMA, LAHTI, 1992).

We can estimate the beam's resonant modes and bending wave propagation velocity in the solid from the system's IR analysis performed at the measurement points. Moreover, our approach will allow us to not only execute a temporary check of the structure but also to observe how the structure interacts with the fluid surrounding it (MAO, PIETRZKO, 2013).

The structure tested consisted of beams made of a sandstone material called *Bateig*, manufactured in the province of Alicante. We selected this material because its mechanical properties are similar to those used in the building sector and can, therefore, be used as a reference in related studies.

Finally, our lab results obtained in the frequency domain are compared to those obtained in the modal analysis applying the Euler-Bernoulli free-free boundary condition model and the FEM-model, and our bending propagation velocity calculation to that obtained from the Euler-Bernoulli and Timoshenko's approximations, and they show a very close agreement.

2. Background theory

2.1. Bending waves in beams

In beams bending waves generate a flexural motion responsible for sound radiation. This flexural motion has been described in (HAN *et al.*, 1999) through four approximations, namely Euler-Bernoulli, Rayleigh, Shear and Timoshenko. They solve the trans-

verse motion equation for beams to yield the natural frequencies and Eigen functions if the following six assumptions are observed:

- 1) the beam's material is linear straight and elastic,
- 2) the beam's Poisson effect is disregarded,
- 3) the beam's cross-section area is symmetric with respect to its flexural axis,
- 4) the beam's planes are perpendicular to the neutral axis and remain so after deformation,
- 5) the beam's angle of rotation is such that the small angle assumption applies,
- 6) the beam's axial direction is considerably longer than the other two dimensions.

Assumption 6 is readily solved once the slenderness ratio, S_l , is calculated by Eq. (1)

$$S_l = L\sqrt{\frac{A}{I_y}}, \quad (1)$$

where L refers to the length of the beam [m], A to its cross-section area [m²], and I_y to the mass moment of inertia of its cross-section area with respect to the y axis (its flexural axis) [m⁴]. For instance, for a beam with a rectangular cross section, $A = wh$ and $I_y = wh^3/12$, where w and h correspond to the width and the height of cross section, respectively.

Depending on the slenderness of the beam, a different approach can be taken. If the beam's slenderness is $S_l < 100$, the Timoshenko's model (MAO, PIETRZKO, 2013), offers the best approximations to its vibrational behaviour. This model considers the shear distortion and the rotary inertia effects, which have as great impact on wavelengths as on the thickness of the material. Here the beam's bending wave propagation velocity, c_B [m/s], is given by (COMSOL, 2001)

$$c_B = \sqrt{\frac{\sqrt{\left(\frac{EI_y}{KAG} - \frac{I_y}{A}\right)^2 \omega^4 + 4\frac{EI_y}{\rho A} \omega^2 - \omega^2 \left(\frac{EI_y}{KAG} + \frac{I_y}{A}\right)}}{2\left(1 - \omega^2 \frac{I_y \rho}{KAG}\right)}}, \quad (2)$$

where E is the Young modulus [N/m²], KAG is the shear factor – the product of the cross-section area; A , the shear modulus G [N/m²] and the correction factor K – the fraction ratio of the beam's cross section that is subjected to a shear force; I_y/A , the rotary inertia; ω , the angular frequency [rad/s] and ρ the density of the material [kg/m³].

If, however $S_l > 100$, the Euler-Bernoulli model, less demanding than the Timoshenko's, may be applied. This analytical model greatly simplifies the calculation of the natural frequencies and vibration modes. Here the bending wave propagation velocity in the beam, c_B , is given by:

$$c_B = \frac{\omega}{k} = \sqrt{\omega^4 \frac{EI_y}{\rho A}}. \quad (3)$$

For the simplicity offered, in a first instance, we selected the Euler-Bernoulli model to briefly describe the transverse displacement of the beam, which we proceeded as follows: we chose a continuous slender beam and subjected it to a vibrating motion in the XZ plane. We assumed that the transverse section was flat and perpendicular to the deformed longitudinal axis, and that both the shear deformation and the rotational inertia of the cross section – which we compared to the bending deformation and translational inertia, respectively – were negligible. Figure 1 depicts the flexural motion of a thin beam exhibiting a rectangular cross section subjected to a vibrating force in the XZ plane.

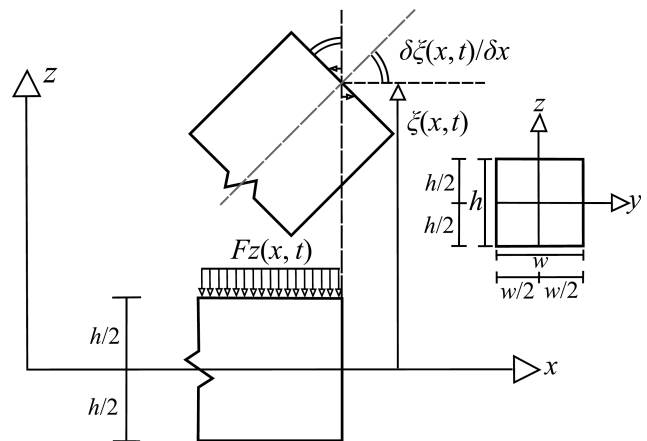


Fig. 1. Flexural motion of a thin beam with rectangular cross-section when subjected to a force in the XZ plane.

By computing the kinetic and potential energies, and adopting the variational principle (FAHY, GARDONIA, 2007), we can obtain the Euler-Bernoulli equation for the lateral displacement $\xi(x,t)$ of a time-dependent harmonic force (CROCKER, 2007) as:

$$-F_z(x, t) = EI_y \frac{\partial^4 \xi(x, t)}{\partial x^4} + \rho A \frac{\partial^2 \xi(x, t)}{\partial t^2}, \quad (4)$$

where $F_z(x, t)$ is the applied force per unit length. The general solution for Eq. (4) when $F(x, t)$ equals zero is

$$\xi(x, t) = \left[\check{A}e^{-jk_b x} + \check{B}e^{jk_b x} + \check{C}e^{-k_b x} + \check{D}e^{k_b x} \right] e^{j\omega t},$$

where k_b is the bending wave number $k_b = \sqrt[4]{\frac{\omega^2 \rho A}{EI_y}}$ [rad/m] and \check{A} , \check{B} , \check{C} , \check{D} are the amplitudes of the different types of waves.

The expression above implies the existence of two different types of waves in the solution. Indeed, the first two terms describe the bending wave propagation in the X positive and negative directions without attenuation. The second two terms, on the other hand, describe non-propagation waves, also known as evanescent waves, the amplitudes of which diminish.

Establishing the free-free boundary conditions in the above expression, the natural frequencies of the beam, f_n , are given by:

$$f_n = \frac{d_n^2}{2\pi L^2} \sqrt{\frac{EI_y}{\rho A}}, \quad (5)$$

where d_n are the roots from the equation: $\cos d_n \cdot \cosh d_n - 1 = 0$, being $d_n = k_{b,n}L$, $k_{b,n}$ is the bending wave number [rad/m] and n the modal index. These frequencies denote which modes are significant for the study of the movement of the beam-type system.

The bending waves in solids, unlike sound waves in the air, are dispersive, meaning that the propagation velocity c_B depends on frequency (CROCKER, 2007). The frequency of the bending wave whose velocity is the same as the propagation velocity for the longitudinal waves in the air is known as the critical frequency, f_c , and is given by:

$$f_c = \frac{c_{\text{air}}^2}{\sqrt{3}hc_L}, \quad (6)$$

where c_{air} is the sound velocity in the air 343 m/s and c_L is the longitudinal wave propagation velocity in the solid $c_L = \sqrt{E/\rho}$ [m/s]. In beams, the acoustic radiation is highly efficient around the critical frequency, whereas below that frequency, the radiation is negligible (GERGES, ARENAS, 2010).

In fact, for the frequency range below the critical frequency, the acoustic impedance (ratio between acoustic pressure and velocity of particle) of the waves is imaginary and positive, therefore the load of the fluid can be considered inertial (like an acoustic mass), and in consequence radiated sound power is negligible. When the bending wave velocity and the propagation velocity in the fluid coincide, the impedance tends to infinite, and the radiation efficiency is maximum. Finally, for those frequencies above f_c where the bending wave propagation velocity is higher than c_{air} , the impedance is real and purely resistive and sound radiation occurs.

On the other hand, according to modal analysis approach (for harmonic free vibration), the displacement of structure can be separate in space and time (LIU, 2015):

$$\xi(x, t) = \phi(x)q(t), \quad (7)$$

where $\phi(x)$ and $q(t)$ are the structural mode shape and the modal coordinate, respectively.

The application of the variable separation technique leads to a set of functions, $\phi_n(x)$ for the structural mode shape and for modal coordinates, $q_n(t)$, which depend on boundary and initial conditions to which the beam is subjected.

Because the mode shapes are orthogonal to each other, the displacement response of the beam at any

arbitrary point can be expressed as a linear combination of these mode shape functions:

$$\xi(x, t) = \sum_{n=1}^{\infty} \phi_n(x, y)q_n(t), \quad (8)$$

and the velocity

$$v(x, t) = \phi_n(x, y)\dot{q}_n(t), \quad (9)$$

where $\phi_n(x, y)$ is the n -th structural mode shape and $\dot{q}_n(t)$ is the modal velocity.

If the medium is discretized, the above equation can be written in a matrix form

$$v = [\phi]q, \quad (10)$$

where $[\phi]$ is a real orthonormal matrix, and $[\phi]^H = [\phi]^T$ (where superscript H denotes the complex conjugate transpose and T denotes transpose).

Acoustic radiation is one of the consequences of the structural motion associated with bending waves in solid objects. The study of structure motion associated radiation is of high practical importance when designing and controlling noise and vibrations in the industry and construction (FAHY, GARDONIA, 2007).

For a beam, assuming it is in an infinite baffle, discretizing the top of the beam surface in differential elements, and using the coordinate system (x, y, z) as shown in Fig. 2, the acoustic pressure can be expressed in terms of the velocity by using Rayleigh's integral

$$p(r) = \frac{j\omega\rho_o}{2\pi} \iint_S v(\bar{r}_o) \frac{e^{-jk|\mathbf{r}-\mathbf{r}_o|}}{|\mathbf{r}-\mathbf{r}_o|} dS, \quad (11)$$

where S is the surface of the beam and

$$\begin{aligned} \mathbf{r} &= (x, 0, z), \\ \mathbf{r}_o &= (x_o, y_o, 0), \end{aligned} \quad (12)$$

$$|\mathbf{r}-\mathbf{r}_o| = \sqrt{(x-x_o)^2 + y_o^2 + z^2},$$

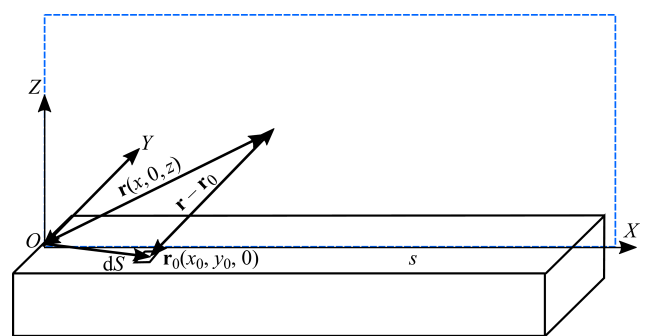


Fig. 2. Schematic diagram of a vibrating beam.

Equation (9) may be included in the Rayleigh integral. To calculate the pressure radiated by a structure according to the vibration modes of a beam:

$$p(\bar{r}) = \sum_{n=1}^{\infty} \frac{j\omega\rho_o}{2\pi} \iint_S \phi_n(x_o)\dot{q}_n(t) \frac{e^{-jk|\mathbf{r}-\mathbf{r}_o|}}{|\mathbf{r}-\mathbf{r}_o|} dS. \quad (13)$$

The contribution of the n -th mode to the pressure in \mathbf{r} is:

$$\frac{j\omega\rho_0}{2\pi} \iint_S \phi_n(x_o)\dot{\eta}(t) \frac{e^{-jk|\mathbf{r}-\mathbf{r}_o|}}{|\mathbf{r}-\mathbf{r}_o|} dS. \quad (14)$$

The contribution of each element dS of the vibrating surface corresponding to the n -th mode to the pressure p in \mathbf{r} is:

$$\frac{j\omega\rho_0}{2\pi} \phi_n(x_o)\dot{\eta}(t) \frac{e^{-jk|\mathbf{r}-\mathbf{r}_o|}}{|\mathbf{r}-\mathbf{r}_o|} dS. \quad (15)$$

2.2. Measurement of the Impulse Response with the Maximum Length Sequence method

For years, several methods in buildings and acoustic measurements have been used in numerous applications. These methods are currently well developed and can achieve acceptable results in most cases. However, there are situations where the signal-to-noise ratio is not high enough and the results obtained are not reliable (STAN *et al.*, 2002).

As discussed above, the MLS technique is commonly used in acoustics and electroacoustics fields. The MLS is a deterministic sequence of pulses (periodic pseudo-random binary sequence consisting of the values between 0 and 1), with a total length $l = 2^m - 1$, where m is the order of the sequence. This signal, treated as a pseudo-random white noise with a negligible DC component, combines the advantages of common excitation techniques for characterizing LTI systems, both transient and steady.

Thus, it can be interpreted as a measurement impulsive technique, without using any pulse. The experimental techniques, presented in the next section, uses MLS signals. This study approximates the beam to a LTI (Linear Time Invariant) system, since the beam motions are small. Also, the system must remain unchanged during the measurement procedure to ensure time-invariance. With this in mind, this method can be considered a very powerful tool to analyse acoustic and vibratory phenomena.

Some precautions must be taken, though, regarding the use of the MLS signal. Firstly, the signal length period must be longer than the impulse response of the device under test (DUT). If this condition is not satisfied, one part of the impulse response signal will be time-aliased. Secondly, as mentioned, the system must be in linear conditions to prevent non-linearities in the system.

2.3. K-Space processing

Part of the signal processing in the experimental procedure was inspired in the Near-field Acoustic Holography (NAH) technique (MAYNARD *et al.*, 1985; WILLIAMS, 1999; SEAN, 2010). As is well known, the

NAH technique implies the measurement of the amplitude and phase of the sound pressure field generated by a source in a parallel plane close to it using an array of microphones. The proposed methodology assumes that the measurement plane matrix is a rectangular grid perpendicular to the bending waves generated by the beam, when subjected to mechanical excitation, making the acoustic field reconstructable.

Additionally, and assuming that the acoustic waves radiated by the beam are mainly propagated in the perpendicular direction to its bending displacement (predominantly k_y), and using a filter in K-Space we can remove those components which are not propagating in that direction (i.e. interfering components from other sources). The advantages and drawbacks of some of these types of filters are discussed in (ESCUADER *et al.*, 2007).

For a two-dimensional surface described by a rectangular coordinate system as shown in Fig. 2, the Spatial Fourier transform for the acoustic pressure and the velocity and their inverse are defined as (WILLIAMS, 1999):

$$P(k_x, k_y) = \iint_{-\infty}^{+\infty} p(x, y) e^{(jk_x x + jk_y y)} dx dy, \quad (16)$$

$$p(x, y) = \iint_{-\infty}^{+\infty} P(k_x, k_y) e^{(-jk_x x - jk_y y)} dk_x dk_y,$$

$$V(k_x, k_y) = \iint_{-\infty}^{+\infty} v(x, y) e^{(jk_x x + jk_y y)} dx dy, \quad (17)$$

$$v(x, y) = \iint_{-\infty}^{+\infty} V(k_x, k_y) e^{(-jk_x x - jk_y y)} dk_x dk_y.$$

We find analogies with the usual Fourier transform for time in the frequency domain.

We can demonstrate, thus, that the radiated sound power of a beam-type structure can be expressed as

$$W(\omega) = \frac{1}{2} \text{Re} \left[\iint_{-\infty}^{+\infty} p(x, y, z=0) \cdot w^*(x, y) dx dy \right], \quad (18)$$

where $*$ denotes the complex conjugate and Re , the real part of a complex value.

By using the Parseval theorem, we can demonstrate that:

$$W(\omega) = \frac{\rho_0 \omega}{8\pi^2} \left[\iint_{-\infty}^{+\infty} \frac{|V(k_x, k_y)|^2}{\sqrt{k^2 - k_x^2 - k_y^2}} dk_x dk_y \right]. \quad (19)$$

Note that $\sqrt{k^2 - k_x^2 - k_y^2}$ is real only if $k^2 \geq k_x^2 + k_y^2$ and the equation can be rewritten as:

$$W(\omega) = \frac{\rho_0 \omega}{8\pi^2} \left[\iint_{k^2 \geq k_x^2 + k_y^2} \frac{|V(k_x, k_y)|^2}{\sqrt{k^2 - k_x^2 - k_y^2}} dk_x dk_y \right]. \quad (20)$$

From the equations we derive that only supersonic waves-wave number components (values of wave number satisfying $k^2 \geq k_x^2 + k_y^2$) radiate to the far-field, and the subsonic wave number components, associated only with decaying near-field waves, do not contribute to the sound radiation in the far-field.

As a summary of this subsection, we can argue that the sound field radiated by any source may be decomposed in an angular spectrum in the K-space (or wave number space) as the superposition of plane waves travelling in different directions. The spatial period of each of these harmonic waves is commonly described by their wavelength. However, the mathematical definition of a wave suggests that its spatial variations are better described by the wavenumber vector $\mathbf{k}(k_x, k_y, k_z)$.

3. Experimental procedure

3.1. Test sample

The proposed methodology uses two rectangular cross-section beams as experimental basis. The specimens were made of a sandstone material called *Bateig*. The physical and mechanical characteristics of the specimen under test are presented in Table 1.

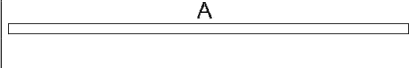

Table 1. Physical and mechanical characteristics of the tested sample (Bateig Stone).

Characteristic	Value
Longitudinal propagation velocity C_L	3718 m/s
Young's modulus E	32 GPa
Shear's modulus G	13 GPa
Poisson's ratio μ	0.230
Density ρ	2312 kg/m ³

The Young's modulus and the Poisson's ratio were calculated under the standard UNE-EN 12390-13 (UNE-EN 12390-13:2014, 2014). Furthermore, the longitudinal propagation velocity was obtained using the transmitter-receiver ultrasonic system (WORKMAN *et al.*, 2007). The Shear modulus (G) was derived from Young's modulus (E). The remaining parameters were obtained from the above Table 1 or by direct measurement. The stone sample was measured and weighted to obtain the density (ρ).

The geometry of the two beam-specimens is shown in the Table 2.

Table 2. Description of the beams' geometry.

Specimen 1: 	$L_{1-A} = 1.17$ m $h_{2-A} = 0.03$ m $w_{2-A} = 0.08$ m
Specimen 2: 	$L_{1-Total} = 1.17$ m $L_{2-A} = 0.53$ m $L_{2-B} = 0.64$ m $h_{2-A} = 0.06$ m $h_{2-B} = 0.03$ m $w_{2-A} = 0.08$ m $w_{2-B} = 0.08$ m

Although the simple supported boundary condition is, in many aspects, desirable for teaching purposes, due to its relatively simple analytic solutions, it is rarely seen in practice. We have selected the free-free boundary conditions (FFBC) for the experimental setup. To emulate FFBC, the beams, as shown in Figs. 3 and 4, were supported with a recycled polymer, because of its low stiffness.

Regarding the boundary conditions of the beam supports, and to verify the validity of the experimental setup, two eigen-frequency 3D numerical models were implemented, using a finite-element software (with COMSOLTM Multiphysics (2001)). In the first model, a FFBC was applied, whereas in the second, the beam was supported by springs, reproducing the actual setting of the experiment.

Table 3 compares the first 8 resonance modes for the Euler-Bernoulli (CROCKER, 2007) beam model in free-free conditions with the two numerical models above mentioned.

Table 3. Frequency response comparison between analytical Euler-Bernoulli solution and two Eigen-frequency 3D-FEM models to the continuous beam.

Bending mode number	Euler-Bernoulli solution [Hz]	FEM modal free-free boundary conditions [Hz]	FEM modal springs boundary conditions [Hz]
1	84.64	85.01	84.85
2	234.90	233.40	232.90
3	455.50	454.70	453.90
4	741.20	745.80	744.30
5	1107.00	1103.00	1103.70
6	1518.00	1524.00	1521.00
7	2004.00	2003.00	2000.00
8	2535.00	2537.00	2567.00

The correlation between the analytical and the numerical data is very high. Therefore, we assume that

the spring boundary conditions can also be considered as free-free. Thus, the experimental setup can be validated.

3.2. Procedure

The experimental configurations are graphically explained in Fig. 3. The first part of the experimental procedure involved the measurement of the beams using accelerometers. The second part consisted in the characterization of the acoustic pressure field radiated by the beams using a microphone. Both measurements share the signal acquisition hardware.

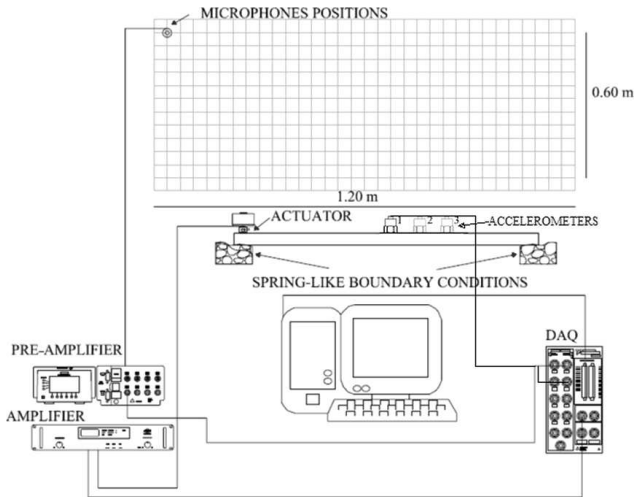


Fig. 3. Configuration of the experimental set-up used for recording the acoustic field.

As already explained, two elastic endings were used to support the beams and thus, simulate a free-free boundary condition. The excitation system consisted of an actuator (Mini-Pro-NXT Fane electro-dynamics actuator 80 MP), typically seen in audio systems called Distributed Mode Loudspeaker (DML). To verify the efficiency of this system, we compared it with standard excitation systems for measuring vibrations, such as a hammer and a shaker. In the results and discussion section, we demonstrate the effectiveness of this system as a vibro-acoustic exciter. Figure 4, top and bottom, shows a detail of the experimental set-up. On the top, we can see the location of the source (actuator) 2 cm away from the left edge of the beam, the boundary conditions and the microphone used to perform the measurement of the field radiated by the beam. On the bottom, we located another actuator in the centre, and three accelerometers near the left edge of the beam.

The test signal was a MLS, whose properties are shown in Table 4.

Specifically, for measurement of vibration purposes, we used three Brüel and Kjær piezoelectric accelerometers, all connected to a preamplifier NEXUS Brüel & Kjær Type 2693-0S4. Each beam was divided in 38



Fig. 4. Detailed view of a section of the experimental setup. Top: location of the source (actuator) 2 cm away from the left edge of the beam. Bottom: three accelerometers near the left edge of the beam and an actuator in the centre.

Table 4. MLS properties.

Variable	Value
Quantization	16 bits
Sample rate f_s	96 kHz
Sequences number	16
Signal duration	3 s
Signal length before average in samples	32 768

parts, obtaining 37 measurement points with a separation Δ of 3 cm.

We registered the acoustic field in a normal plane to the propagation of the bending waves in the structure. The measurements were performed in anechoic conditions and the Brüel & Kjær Type 4951 microphone linked to a NEXUS Brüel & Kjær Type 2693-0S4 pre-amplifier.

For each beam sample we scanned two 60×60 matrices with a $dx = 1$ cm resolution for a total of 3600 points in each matrix. We used two matrices because the robotic arm presents a geometric limitation (not allowing movements above 0.60 m). After capturing the signal, we linked the matrices. Thus, we sampled the acoustic field of each beam with a total of 7200 measurement points.

The captured signal was transmitted to the National Instruments BNC 2110 data acquisition card. This card allowed the automation of the microphone displacement. The microphone was placed on a me-

chanical arm and the actuator, on the upper face of the beam close to one of the ends, specifically at 0.02 m as in the first experimental set-up.

3.3. Signal processing

After we measured the vibration with the accelerometers, we processed the signals to find out the impulse response at each measurement point. From the impulse response (IR), a Fast Fourier Transform (FFT) renders the frequency response of the system. Provided that the MLS signal preserves the phase reference, a temporal analysis will enable us to see pulse propagating in the solid.

Likewise, we processed the pressure field captured by the microphone to derive the IR of the 7200 measurement points. This allowed the visualization of the temporal evolution of the phenomenon and the performance of a frequency analysis. This temporal analysis allows to demonstrate, for instance, the influence of the actuator above the 3 kHz.

In the next section the results of the experiments are explained, once the signal processing had been executed in MATLAB®.

4. Results and discussion

4.1. Experimental validation

The experimental procedure proposed in this work was compared with the traditional techniques (shaker and hammer). In this way, we validate the second experimental set-up through which has served to characterized the behaviour of the beam. Table 5 shows a comparison between the frequency response for a hammer impact, a shaker, and for the actuator for the first eight resonant modes.

Table 5. Frequency response between hammer and the actuator [Hz].

Mode	Hammer	Shaker	Actuator
1	88.0	83.50	87.90
2	225.10	232.90	225.60
2	434.20	440.90	436.60
4	–	745.60	738.00
5	–	1097.00	1087.00
6	1615.00	1513.00	1493.00
7	1826.00	1996.00	1994.00
8	–	2521.00	2441.00

Table 5 shows that the correlation between the techniques is high, meaning that the electroacoustic system proposed parallels the frequency response of the structure with a good performance.

Figure 5 shows the displacement frequency response of the continuous beam using the Mini-Pro-

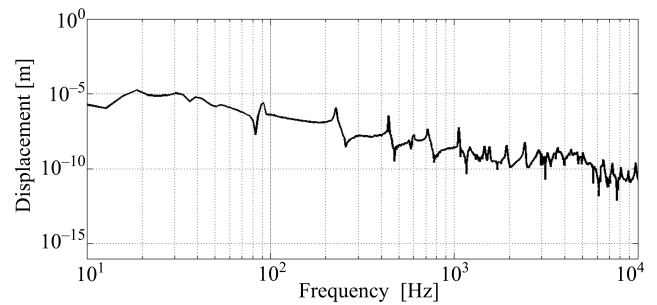


Fig. 5. Displacement frequency response of the continuous cross section beam using the actuator as exciter.

NXT actuator. The analysis of this curve indicates that the technique here presented offers a wider frequency range, being therefore more suitable for the purpose of the present work.

The described experimental setup, with this “low cost actuator”, which can be coupled to the structure, combined with the proper use of pseudorandom sequences (specifically MLS), allows us to have a whole frequency range with a reliable signal-to-noise ratio.

4.2. Frequency response

In a first step, we analysed the spatially average pressure frequency response of those measurement points close to the beam. Figure 6 shows the resulting spectrum, where the critical frequency $f_c = 589$ Hz, analytically calculated from Eq. (5) is highlighted. It establishes the lower frequency limit for the sound radiation to occur.

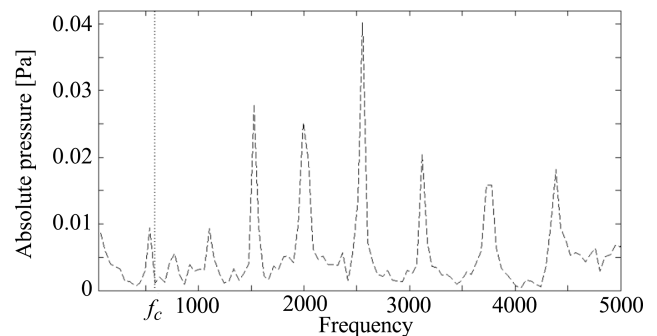


Fig. 6. Spatially averaged pressure frequency response obtained from those measurement points close to the continuous beam.

Figure 6 also identifies the resonance peaks corresponding to the radiation modes. From the analytical solution of the Euler-Bernoulli free-free beam model we evaluated the difference between the measured resonance frequencies and the ten first analytical bending modes (Eq. (4)). The results are also presented in Table 6, where the difference (in %) is the relative percentage deviation of the results obtained from the acoustic field data in relation to the analytical solution.

Table 6. Comparison between experimental contact data and experimental contactless results (vibratory and acoustical).

Bending mode number	Accelerometer [Hz]	Microphone [Hz]	Error [%]
1	88.00	70.00	-20.10
2	233.00	257.00	10.30
3	444.00	539.00	21.40
4	748.00	773.00	3.34
5	1097.00	1102.00	0.46
6	1513.00	1524.00	0.73
7	1994.00	1993.00	-0.05
8	2533.00	2556.00	0.91

The acoustic records of the first three resonant modes are not clearly identifiable because all of them show a high deviation. This may be due to the coincidence phenomenon in an area close to the critical frequency, f_c . Below the f_c , sound radiation is almost nonexistent; near the f_c , sound radiation is highly efficient (FAHY, GARDDONIA, 2007). The deviation in the first mode is due to the position of the force, as is not applied to the centre of the beam, a condition that would facilitate the presence of the first resonance mode. Above the critical frequency, the correlation of the experimental data is very high (differences less than 5%). Therefore, the acoustical experiment is validated. Nevertheless, this alternative experimental procedure can be a useful tool to characterize high radiation resonant modes.

4.3. Vibratory and acoustic response of the structure

The use of MLS signals provides a phase reference for all the vibratory and acoustic signals recorded. This allows us to observe any intended modal form. For instance, Fig. 7 (see Fig. 6 for all modes) shows the

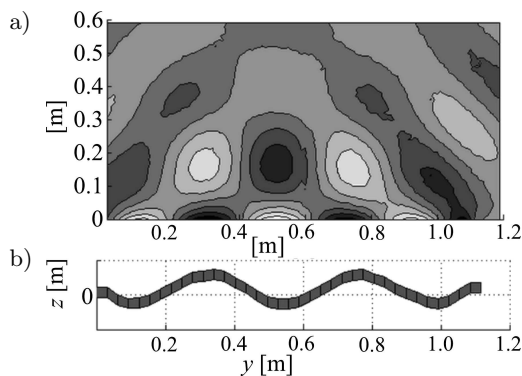


Fig. 7. Vibratory and acoustic results for the continuous beam (5-th mode – 1100 Hz): a) real part of the pressure field radiated by the beam in the window of 1.2×0.6 m, b) modal displacement (relative values).

5-th modal form for the continuous beam. The real part of the pressure field radiated by the beam is shown at the top, and the amplified displacement resulting from the vibration measurement on the structure at the bottom.

Figure 7 also shows a slight displacement of the beam ends in the areas close to the elastic support, confirming the recreation of the free-free condition approach. Consequently, there is an absolute consistency between the vibration mode of the structure and the radiated field by the structure.

Figure 8 shows the 6th mode of the non-uniform cross section beam through the relationship between vibratory and acoustical results.

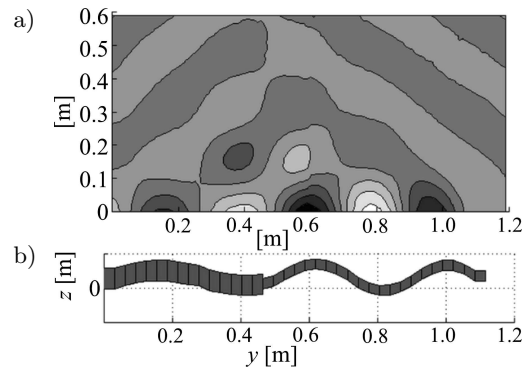


Fig. 8. Vibratory and acoustic results for the non-continuous beam (6-th mode – 1428 Hz): a) real part of the pressure radiated field by the beam in the window of 1.2×0.6 m, b) modal displacement (relative values).

In Fig. 8, we can easily differentiate the mode shape in the pressure field. In the thin (right) portion of the non-uniform cross-section the movement is easier than that in the thick (left) one.

4.4. Temporal analysis

A significant feature of the MLS technique is its ability to synchronize each measurement point and enable the observation of the generated wave fronts, as well as their propagation.

Figure 9 shows specific information regarding the evolution of the wave fronts at the time point

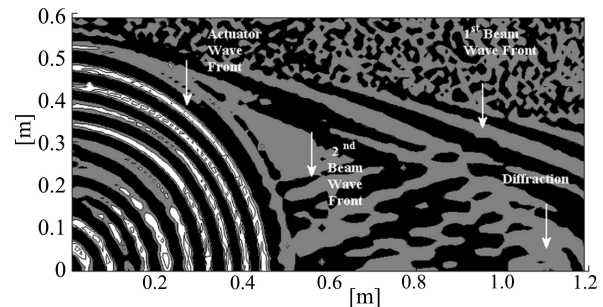


Fig. 9. Wave fronts at the time point 1.6563 ms, obtained after processing the 7200 impulse responses of the records for each point.

1.6563 ms, obtained after processing the 7200 impulse responses of the records for each point.

The figure shows both the wave front generated by the beam and the front generated by the actuator as well as the diffraction at the beam end, on the right side. The wave front generated by the actuator is quasi-spherical, similar to that of a point source, whereas the wave front generated by the beam is flat. The wave front inclination responds to the way the beam has been excited. Note that the actuator is on the left side of the beam. Therefore, there is a delay in the pulse across, resulting in the inclination of the flat wave front. Clearly, the pulse moves at a higher speed through solid elements than through the air. The pulse in the solid element covered the entire length of the beam (1.2 m) and reflected (second wave front), while the pulse in the air only covered half a metre. The temporal behaviour of each mode can be observed by using a band-pass filter.

4.5. K-space analysis

We obtained the spatial distribution of the sound pressure field in the frequency domain (from the phase information for each measurement point and by performing a Fourier transform), as shown in Fig. 10 for the case of 2 kHz. Figure 10a shows that the beam radiation is predominant in the acoustic field, and therefore, the wavelength of the flexural wave in the solid, λ [m], can be calculated from the spatial distance between maximums or minimums of the radiated acous-

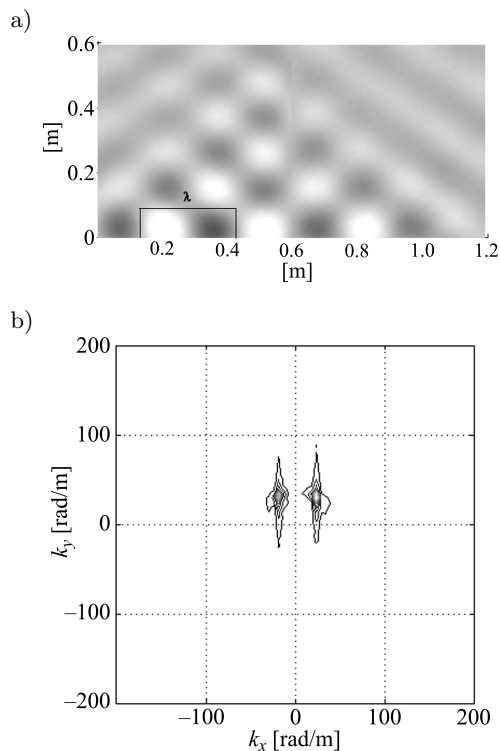


Fig. 10. Sound pressure field at 2 kHz: a) spatial distribution in the measurement grid, b) K-space representation.

tic wave in the x direction close to the upper surface of the beam. For the case of 2 kHz, the value of λ is approximately 0.30 m, as marked out in the Fig. 10a.

The representation in the K-space of the sound pressure field at 2 kHz is shown in Fig. 10b. It was obtained by implementing a 2-D Fourier transform over all the spectral values in the measurement grid and illustrates the spatial frequencies k_x and k_y that conform the spatial frequency k in the measurement plane. As observed, the predominant radiation occurs in the y direction (spatial frequency, k_y), supporting the assumption that sound radiation of the beam is perpendicular to the upper face of the structure.

At frequencies above 3 kHz, the radiation from the beam is masked by the actuator sound radiation. Figure 11 shows, as an example, the sound pressure field at 4 kHz. Figure 11a illustrates how the spherical pattern of sound radiation of the actuator and of the beam are significantly overlapped, making it difficult to properly analyse the radiation of the beam as previously.

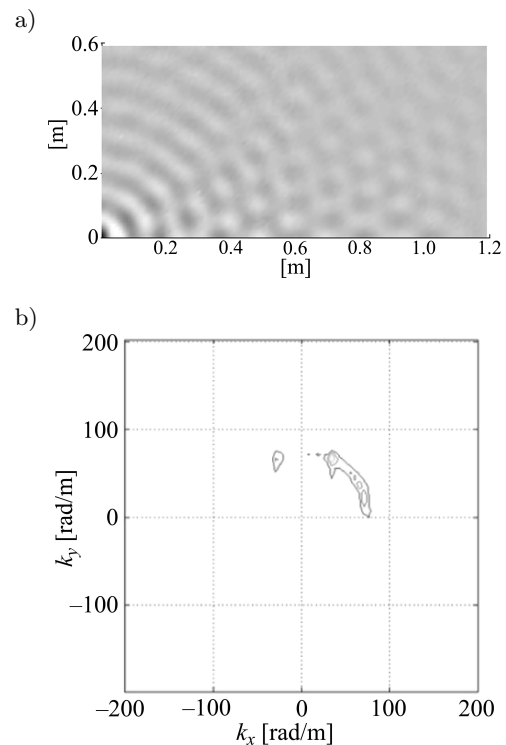


Fig. 11. Sound pressure field at 4 kHz (sound radiation overlapping of the actuator and the beam): a) spatial distribution in the measurement grid, b) K-space representation.

The representation in the K-space in Fig. 11b verifies the predominance of k_x components in the sound pressure field. As stated and illustrated in Fig. 10, the beam sound radiation is normal to its upper surface (k_y components).

In order to minimize this interfering sound radiation, a filter in the K-Space was applied to remove the spectral components generated by the direct radiation of the actuator and to better study the radiation of

the beam itself. The filter used was a Veronesi filter (VERONESI, MAYNARD, 1987; 1989), which is commonly employed in NAH applications. This filter response in K-space, $H_v(k_x, k_y)$, can be expressed as:

$$H_v(k_x, k_y) = \begin{cases} 1 - 0.5e^{-(\frac{k}{k_c}-1)/s} & k \leq k_c, \\ 0.5e^{-(\frac{k}{k_c}-1)/s} & k > k_c, \end{cases} \quad (21)$$

where k_c and s are the spatial cut-off frequency and the filter slope respectively. Figure 12 shows the response in K-space of the Veronesi filter (VERONESI, MAYNARD, 1989).

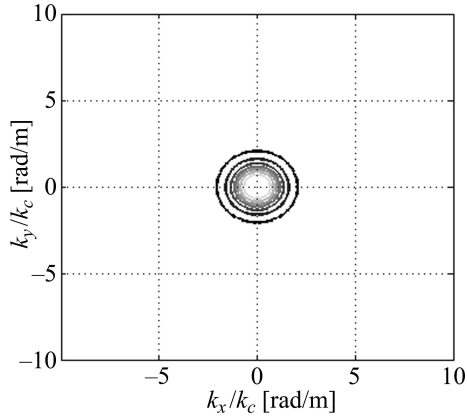


Fig. 12. Iso-lines representing the response in K-space of the Veronesi filter ($s = 0.65$).

Once the filtering procedure was carried out, an inverse 2-D Fourier transform was performed in order to return back to the frequency domain.

In Fig. 13a, the resulting filtered sound pressure field at 4 kHz is shown (in this case, the filter parameters were $k_c = 45$ and $s = 0.65$). Note that the contribution of the beam’s sound radiation of the beam to the acoustic field can be analysed more accurately since the k_x components from the radiation of the actuator have been minimized. This enabled us to estimate the

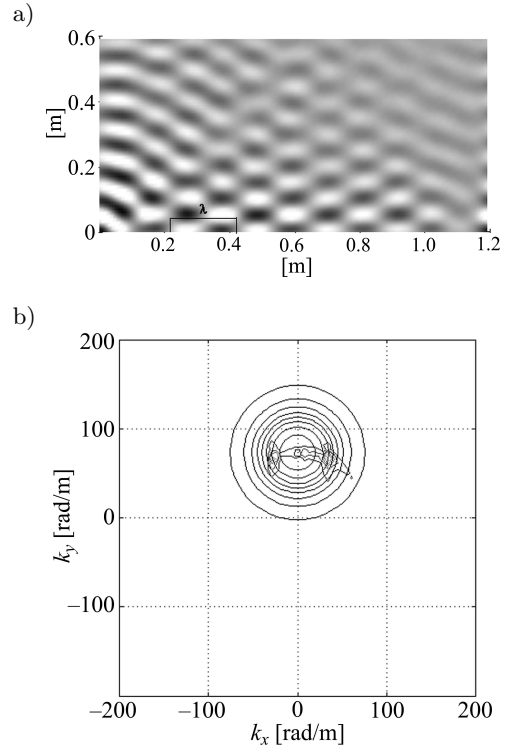


Fig. 13. Filtered sound pressure field at 4 kHz: a) spatial distribution in the measurement grid, b) K-space representation (Veronesi filter iso-lines are included).

wavelength λ of the flexural wave in the solid, which for the case of 4 kHz is approximately 0.20 m.

Figure 13b shows the resulting filtered representation in the K-space. The cut-off region of the Veronesi filter can be also identified as iso-lines.

Using the previous methodology, we obtained the value of λ of several frequencies with the aim of calculating the experimental bending wave propagation velocity of the beam, c_B . Figure 14 shows the comparison of the c_B obtained with the proposed methodology and the Euler-Bernoulli free-free beam model (using Eq. (3)).

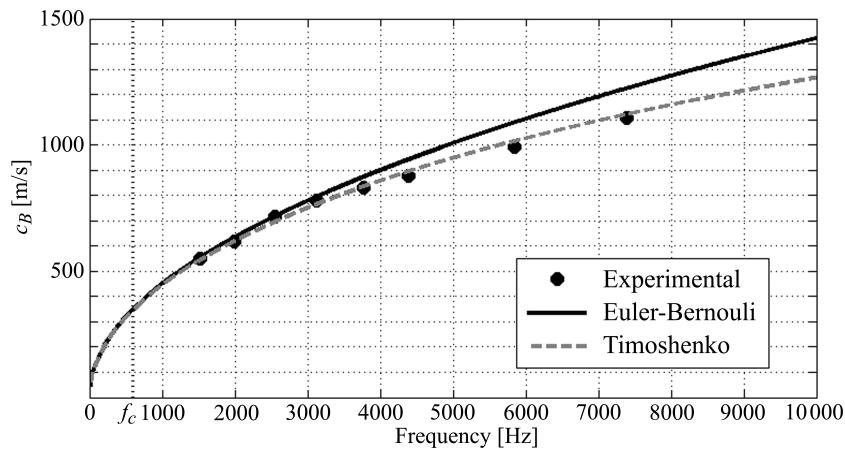


Fig. 14. Bending waves propagation velocity obtained experimentally, and with the Euler-Bernoulli and Timoshenko models.

The c_B calculated using the Timoshenko free-free beam model (Eq. (2)) was also included, fitting better to the experimental results. It must be reminded that the Timoshenko model takes into account the resistance to shear deformation and the rotary mass inertia and in consequence outcome effect in the calculus for those wavelengths comparable with the thickness of the beam. Figure 14 also marks out the critical frequency f_c . It is important to highlight that the value of this frequency is almost the same (around 589 Hz) for the analytical solution and the proposed alternative experimental methodology.

5. Conclusions

An experimental procedure has been put forward for studying the vibro-acoustic behaviour of beam-type structures based on the use of Maximum Length Sequence (MLS)-type pseudorandom signals. In comparison to other techniques, this method requires a relatively simple post-processing procedure with a high signal-to-noise ratio. This technique has proved efficient as an alternative to characterise the vibratory and radiation field of this type of structures. The only precaution to be taken consists of limiting the testing signal so as to avoid nonlinearities.

The presented procedure may be very useful in many acoustical engineering fields, specifically to beams, plates and compound structures, where it is mandatory that the use of prototypes have the dimensions required, usually smaller than real size, for laboratory testing.

References

- BERANEK L., MELLOW T. (2012), *Acoustics: Sound Fields and Transducers*, Oxford: Academic Press.
- COMSOL Multiphysics (2001), COMSOL Documentation CFD Module, Version 4.3.
- CROCKER M.J. (2007), *Handbook of noise and vibration control* (M.J. Crocker, Ed.), New York: John Wiley & Sons.
- ELLIOT S.J., JOHNSON M.E. (1993), *Radiation modes and the active control of sound power*, Journal of the Acoustical Society of America, **94**, 4, 2194–2204.
- ESCUDE E., ALBA J., RAMIS J. (2007), *Study of the parameters of the wiener filter in near-field acoustic holography* [in Spanish: *Estudio de los parámetros del filtro wiener en near-field acoustic holography*], Int. Mét. Num. Cál. Dis. Ing, **23**, 2, 189–203.
- EWINS D.J. (1984), *Modal testing: theory and practice*, New York: John Wiley and Sons.
- FAHY F., GARDONIA P. (2007), *Sound and structural vibration, radiation, transmission and response* (2nd ed.), Oxford: Academic Press.
- GERGES S., ARENAS J. (2010), *Fundamentals and noise and vibrations control* [in: Spanish: *fundamentos y control del ruido y vibraciones*] (2nd ed.), Florianópolis: NR Editora.
- HAMBRIC S.A. (2006), *Structural acoustics tutorial – Part 1: Vibrations in structures, acoustic today*, Journal of the Acoustical Society of America, **2**, 4, 21–33.
- HAN S.M., BENOROYA H., WEI T. (1999), *Dynamics of transversely vibration beams using four engineering theories*, Journal of Sound and Vibration, **225**, 5, 935–988.
- LINJAMA J., LAHTI T. (1992), *Estimation of bending wave intensity in beams using the frequency response technique*, Journal of Sound and Vibration, **153**, 1, 21–36.
- LIU A.N. (2015), *Vibro-acoustics*, Volume 1, 2nd ed., Berlin Heidelberg: Science Press, Beijing and Springer-Verlag.
- MAO Q., PIETRZKO S. (2013), *Control of noise and structural vibration. A MATLAB®-Based Approach*, London: Springer.
- MAYNARD J.D., WILLIAMS E.G., LEE Y. (1985), *Near-field acoustic holography I. Theory of generalized holography and the development of NAH*, Journal of the Acoustical Society of America, **78**, 1395–1413.
- MAZUREK R., LASOTA H. (2007), *Application of maximum-length sequences to impulse response measurement of hydroacoustic communication systems*, Hydroacoustics, **10**, 123–130.
- MCCONNELL P. (2000), *Transducer inertia and stinger stiffness effect on FRF measurements*, Mechanical Systems and Signal Processing, **14**, 4, 625–636.
- RIFE D.D., VANDERKOOY J. (1989), *Transfer-function measurement with maximum-length sequences*, Journal of the Audio Engineering Society, **37**, 6, 419–444.
- SCHROEDER M. (1979), *Integrated-impulse method measuring sound decay without impulses*, Journal Acoustics Society of America, **66**, 2, 497–500.
- SEAN F.W. (2010), *Techniques for implementing near-field acoustical holography*, Sound and Vibration, **44**, 2, 12–16.
- STAN G.-B., EMBRECHTS J.-J., ARCHAMBEAU D. (2002), *Comparison of different impulse response measurement techniques*, Journal Audio Engineering Society, **50**, 4, 249–262.
- SUNG C.C., JAN J.T. (1997), *The response of and sound power radiated by a clamped rectangular plate*, Journal Sound and Vibration, **207**, 3, 301–317.
- SZWERC R.P., COURTNEY B.B., HAMBRIC S.A., TIMOTHY E. (2000), *Power flow in coupled bending and longitudinal waves in beams*, Journal of the Acoustical Society of America, **117**, 6, 3186–3195.
- UNE-EN 12390-13:2014 (2014), *Testing hardened concrete – Part 13: Determination of secant modulus of elasticity in compression*.
- VANDERKOOY J. (1994), *Aspects of MLS measuring systems*, Journal of the Audio Engineering Society, **43**, 219–231.

25. VERONESI W.A., MAYNARD J.D. (1987), *Near-field Acoustic Holography (NAH) II. Holographic reconstruction algorithms and computer implementation*, Journal of the Acoustical Society of America, **81**, 5, 1307–1322.
26. VERONESI W.A., MAYNARD J.D. (1989), *Digital holographic reconstruction of sources with arbitrarily shaped surface*, Journal of the Acoustical Society of America, **85**, 2, 588–598.
27. VÖRLANDER M., KOB M. (1997), *Practical aspects of MLS measurements in building acoustics*, Applied Acoustics, **52**, 3, 239–258.
28. WILLIAMS E.G. (1999), *Fourier acoustics. Sound and near-field acoustical holography*, London: Academic Press.
29. WORKMAN G., KISHONI D., MOORE P. (2007), *Nondestructive Testing Handbook. Vol. 7, Ultrasonic Testing*, Columbus, OH, USA: ASTN.